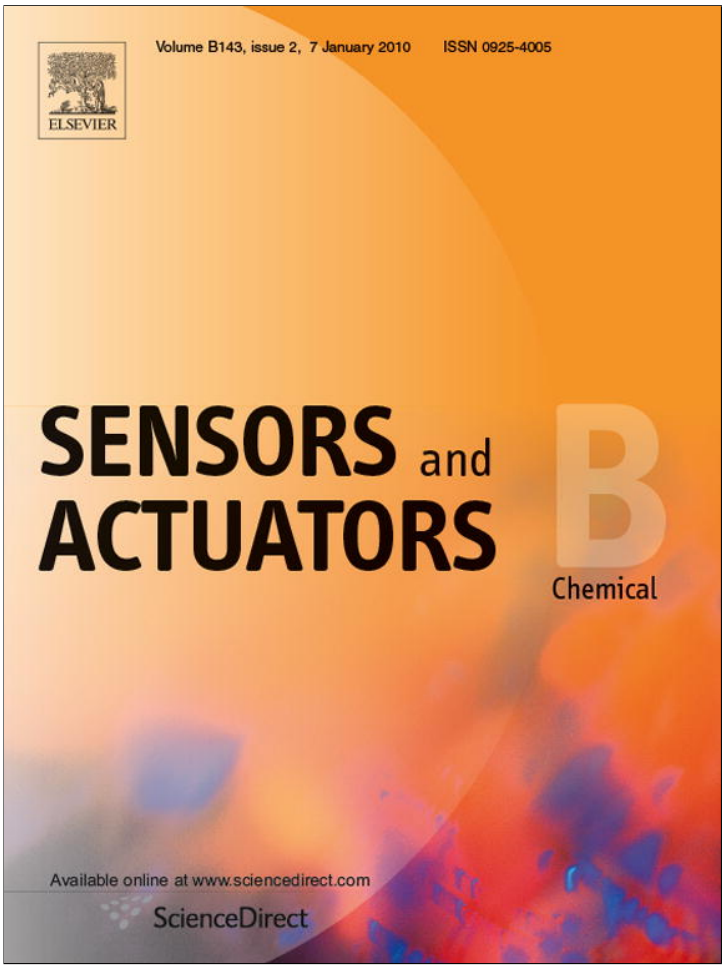

Sensors and Actuators B 143 (2010) 795–798

Contents lists available at ScienceDirect

Sensors and Actuators B: Chemical

journal homepage: www.elsevier.com/locate/snb

Short communication

Evidence shows concentration polarization and its propagation can be key factors determining electroosmotic pump performance

Daniel G. Strickland, Matthew E. Suss, Thomas A. Zangle, Juan G. Santiago*

Department of Mechanical Engineering, Stanford University, Stanford, CA 94025, USA

ARTICLE INFO

Article history:
Received 20 August 2009
Received in revised form
30 September 2009
Accepted 4 October 2009
Available online 12 October 2009

Keywords:
Electroosmotic pump
Electrokinetic pump
Concentration polarization
Duhkin number
Nanochannel
Surface conduction

ABSTRACT

Porous structures with submicron pore diameters and low ionic strength electrolytes yield more efficient electroosmotic (EO) pumps. For these conditions, however, electric double layers may carry a substantial portion of ionic current, creating an imbalance between current carried by anions versus cations. This leads to the formation of net neutral regions of ion depletion and enrichment on opposite sides of the pump. We visualize ionic concentration enrichment and depletion using a custom visualization setup with an embedded porous glass EO pump. Visualizations and conductance measurements indicate that concentration polarization (CP) zones are formed and propagate in EO pump systems with order 100–1000 μM ionic strength. To date, no EO pump model has taken CP into account and yet CP has a significant effect on pumping rate and power consumption. We propose pore-volume-to-surface-area ratio as a new Duhkin number length scale for predicting CP regimes in EO pumps. CP and its propagation can have profound and long-range effects on ionic conductivity and electric fields in EO pumps.

1. Introduction

Electroosmotic (EO) pumps can potentially provide a large range of flow rates and pressure capacities, have no moving parts, and have a high self-pumping frequency [1,2]. A simple EO pump consists of a porous substrate (often glass), two electrodes, and a power source. Electrodes are used to create an electric field which imposes a Lorentz force on mobile counterions of electric double layers (EDL) to create bulk fluid flow [2]. EO pumps have been applied in fuel cells [3,4], high pressure liquid chromatography [5], and drug delivery [6]. Challenges to EO pump implementation include achievement of low applied voltage and high flow rate per power, and the effects of electrolysis bubbles [7–10]. These challenges drive designs to pore radii of order of 100 nm [11–13].

When electric fields are applied to systems which incorporate submicron channels, net neutral concentration enrichment and depletion regions may form at interfaces with larger channels; an effect called concentration polarization (CP) [14]. We show CP schematically in Fig. 1. The effects of surface conduction on stationary CP have been modeled and experimentally studied for over 40 years [15]. CP has been visualized experimentally in systems containing nanochannels [16,17], mesoporous beads [18,19], packed beads [20] and porous monoliths [20,21]. In addition, Postler et al. [22] developed a numerical model for electroosmosis in submicron channels which captures CP onset and the effect of adverse pressure loads.

In some cases, CP can propagate and induce strong, system-wide spatiotemporal variations in ionic strength [16,23]. To the best of our knowledge, propagating CP has not been confirmed experimentally in EO pump operation, and models of EO pumps with order 100 nm pore radii do not account for CP [11,12,24]. In this work, we therefore document and study the propagation of CP in an EO pump system. We present visualizations and conductance measurements which confirm experimentally the occurrence of propagating CP in an EO pump with mean pore diameter of order 100 nm. Our intent is to provide compelling evidence that propagating CP is important in EO pump performance and motivate studies which investigate CP in EO pumping.

2. Theory

CP arises when mobile EDL counterions carry a significant portion of the total ionic current. In an EO pore, the associated flux imbalance between co- and counter-ions results in net neutral ion enrichment and depletion downstream and upstream of the pump, respectively. CP can be characterized by a Dukhin number, a surface-to-bulk conductance ratio of the form [16,23,25]:

$$Du \equiv \frac{\sigma_{surf}}{\sigma_{bulk} l} = -\frac{s\upsilon_1 z_1}{F z_1 c_r (\upsilon_1 z_1 - \upsilon_2 z_2)(r/2)}. \quad (1)$$

* Corresponding author at: 440 Escondido Mall, Bldg 530, Rm 224, Stanford, CA 94025, USA. Tel.: +1 650 723 5689; fax: +1 650 723 7657.
E-mail address: juan.santiago@stanford.edu (J.G. Santiago).

0925-4005/$ – see front matter © 2009 Elsevier B.V. All rights reserved.
doi:10.1016/j.snb.2009.10.005

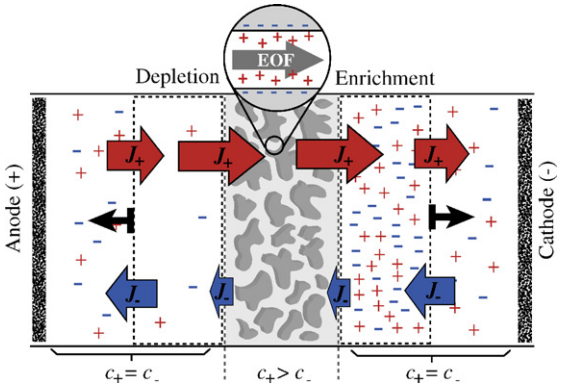

Fig. 1. Schematic of propagating CP in an electroosmotic pump device. System consists of a porous glass structure (grey), connecting channels, and electrodes. Top zoom view depicts the flow through a single pore with direction of electroosmotic flow (EOF) indicated by the grey arrow. When in contact with water, pore walls deprotonate to form EDLs of negative stationary wall charges and diffuse mobile cations. Pores contain an increased cation concentration (c_+) and there are more mobile cations than anions. Electromigration and advection of charge both cause a net cationic flux (J_+) significantly greater than anionic flux (J_-). (Here J is the total ion flux of a species due to electromigration, advection, and diffusion.) A control volume analysis (dashed boxes) indicates net flux of total (positive plus negative) charge into the cathode side and out of the anode side regions. These regions of net ion accumulation and depletion are sufficiently far from wall charge (at least a few Debye lengths away) and so they are approximately net neutral. In some cases, the resulting ion enrichment and depletion zones propagate as concentration shocks (black arrows) and can therefore have long-range spatial effects on concentration distribution [16,23].

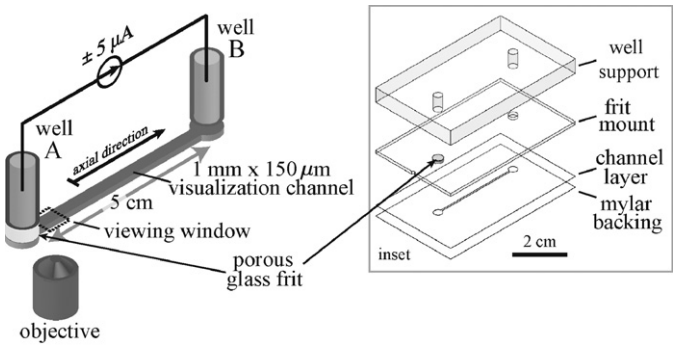

Fig. 2. Experimental setup used to visualize CP and measure channel conductance. The pump substrate is located just below reservoir A, and the view area of the channel is several millimeters past reservoir A. The inset shows the microfluidic chip design.

Here, σ_{surf} and σ_{bulk} are surface and bulk conductance, and l is a characteristic length [25]. s is the surface charge density, c_r is initial electrolyte concentration, υ is ionic mobility, z is ionic charge, r is characteristic pore radius, and F is Faraday's constant. Subscripts 1 and 2 denote counter- and co-ion of the binary electrolyte, respectively. We temporarily use $r/2$ for l, consistent with recent CP literature [23],[1] but further discuss this scale below. Optimized EO pump designs require submicron pores and low ionic strength electrolytes [2,9,13], which result in order unity or higher Du (e.g., 200 nm pore radius silica pump using 1 mM ionic strength has Du of approximately unity).

In some cases, concentration enrichment and depletion zones propagate outwards as shocks. As predicted by Mani et al. [23] and experimentally verified by Zangle et al. [16], propagation is governed by two non-dimensional parameters: a Dukhin number and a co-ion electrophoretic mobility normalized by electroosmotic mobility. When CP propagates, the depletion zone travels upstream against bulk flow, and the enrichment zone propagates downstream. In non-propagating CP, these zones remain local to nanochannel interfaces.

3. Materials and methods

Fig. 2 shows a schematic of the experimental setup. The device consists of (from A to B) a platinum wire electrode and 3.0 mL well, porous glass frit ("frit" is a term describing a glass filter disc made from sintered glass granules) with 450 nm median pore diameter (EoPlex, Redwood City, CA), 1 mm × 150 μm × 5 cm visualization channel, and a second electrode and 3.0 mL well. We galvanostatically controlled all experiments at 5 μA DC using a Keithley Sourcemeter (Cleveland, OH), with positive current defined when reservoir A is at high potential. Our chip's layers are, from bottom to top, a transparent mylar backing, mylar channel layer, acrylic frit mount, and acrylic well support.

We captured images using an inverted epifluorescence microscope (Nikon Eclipse TE300), mercury bulb light source, epifluorescent filter cube, 5×, 0.1 NA objective, and 1.3× demagnifier. We used 10 μM Alexa Fluor 488 succinimidyl ester (Molecular Probes, Eugene, OR) to visualize ionic concentration, and sodium tetraborate decahydrate (Mallinckrodt, Hazelwood, MO) buffer to set ionic strength.

4. Results

4.1. Depletion and enrichment visualization

We performed visualization experiments using 100 μM borate buffer (a very weak buffer with measured pH of 6.8). We here give the concentration of all borate buffers used as the Na^+ concentration, where a mole of sodium tetraborate (borax) dissolves to form two moles of Na^+. For our conditions, we can accurately assume that the concentration of tetraborate (divalent buffering ion) is approximately equal to one half the concentration of Na^+. Measured conductivity and pH values of all buffers used are given in Table S-1 of the supporting materials. In all cases, we used applied currents of +5 and −5 μA. Fig. 3 shows spatiotemporal plots of ion concentration measurements, where we plot transverse-averaged Alexa Fluor intensity versus axial distance and time. The data show concentration depletion and enrichment on the upstream (high potential) and downstream (low potential) sides, respectively, as expected from CP models [16,23]. In the depletion case, ion concentration decreased by an order of magnitude within 90 s. We observed propagation of a depletion concentration front with an approximate front velocity of 400 μm/s. In the enrichment case, characteristic time scales were significantly longer and axial concentration gradients very diffuse; so we were unable to identify clearly an enrichment front or propagation velocity. The final measured enrichment factor was ~1.9.

4.2. System conductance

The potential applied at the electrodes is dropped primarily across the viewing channel [26]. We therefore measured applied potential at constant current to characterize variations in viewing channel conductance. When enrichment or depletion zones propagate into the channel, conductance respectively increases and decreases. Fig. 4 shows conductance measurements for borate concentrations of 100 and 150 μM (measured pH = 6.8 and 6.9, respectively), and applied currents of −5 and +5 μA. For both buffer

[1] Mani et al. [11] presented a Dukhin number with $l = h/2$ (the half height of an infinitely wide channel). A cylinder with diameter h (e.g. an EO pump pore) has twice the perimeter-to-area ratio as an infinitely wide channel of height h and so we use $l = r/2$ for comparisons.

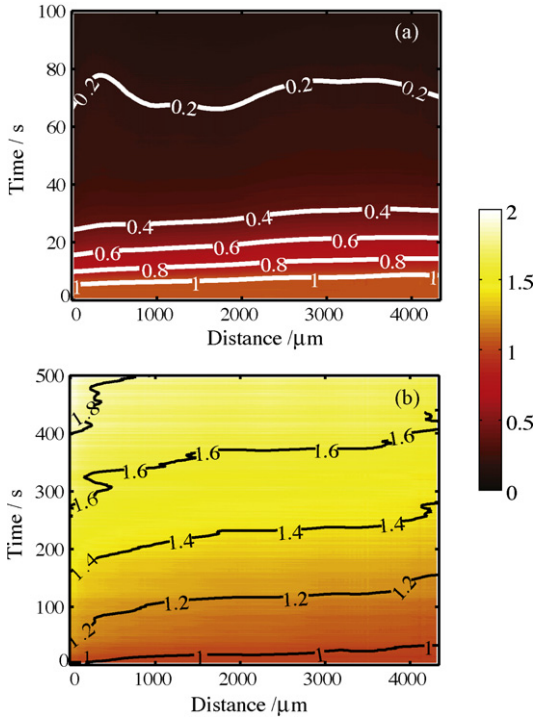

Fig. 3. Spatiotemporal plots of ion concentration enrichment factor versus axial distance from pump-side of viewing window and time. The color intensity data shown is unfiltered, raw data. The contours are based on data convolved with a two-dimensional Gaussian with 15 s and 300 μm widths. (a) Applied current of −5 μA. Data show propagating concentration depletion zone, with front velocity of ~400 μm/s. (b) Applied current of +5 μA. Data show enrichment zone propagation. Concentration reached a final enrichment factor of ~1.9. The enrichment front was significantly more diffuse than the depletion front (this is more clearly apparent in the movies included in the supporting materials).

concentrations, conductance respectively decreased and increased for negative and positive applied current. This is consistent with the visualized concentration changes, and a confirmation of CP propagation. Conductance versus time measurements also highlight the long-range effects of CP. For the 100 μM depletion case, conductance did not stabilize until ~1400 s (reaching 95% of final value). This indicates the depletion zone (with velocity of 400 μm/s) propagated through the 5 cm length visualization channel and into the upstream well.

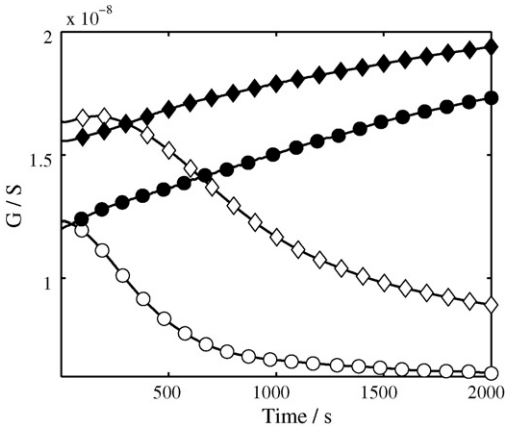

Fig. 4. Measurements of channel conductance (G) in time for applied currents of −5 μA (open symbols) and +5 μA (closed), and borate concentrations of 100 (●) and 150 μM (♦). For both −5 μA cases, conductance decreased to approximately 50% of the initially measured value. For both +5 μA cases, conductance change was more moderate, and increased by up to ~50% (for 100 μM) over the full 2000 s observation period. We attribute these results to depletion zone (former) and enrichment zone (latter) propagation into the visualization channel. This is consistent with visualizations shown in Fig. 3, and is a strong confirmation of propagating CP in our EO pump system.

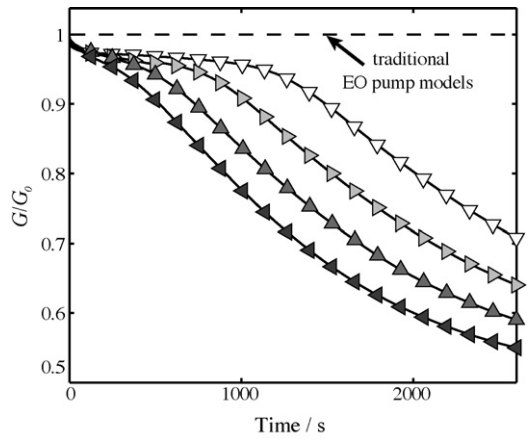

Fig. 5. Measured conductance transients for borate buffer concentrations of 700 (◂), 800 (▲), 900 (△) and 1000 μM (▽). We normalized conductance by the initial measured value. The dashed line represents conductance predicted by traditional EO pump models, which assume constant spatial and temporal ionic strength distributions. Characteristic time scales of transients increased with increasing initial concentration. For all cases, results indicated propagating CP, although calculations of Duhkin number using mean pore radius predict non-propagating CP.

Characteristic time scales of conductance transients were significantly longer for the 150 μM cases, where depletion-case conductance stabilized at ~1900 s. We attribute this to the reduced *Du* associated with the increased initial ionic strength.

4.3. Propagating CP at higher ionic strength

We measured depletion-case (−5 μA applied current) conductance transients at higher borate buffer concentrations. Fig. 5 shows conductance measurements for four borate concentrations from 700 to 1000 μM. As with the lower concentrations, the characteristic time scale of transients increased with increasing concentration.

Even at 1 mM ionic strength, CP induces long-range concentration changes. If we use median pore diameter to calculate *Du*, the model of Mani et al. [23] predicts non-propagating CP at these higher borate concentrations. However, predictions for porous media are not straightforward. For example, from porosimetry data (Porous Materials Inc., Ithaca, NY) of a similar porous glass sample, ~25% of the pore volume should be composed of pores small enough to be within the propagation regime. We hypothesize that the total pore-volume-to-surface-area ratio may instead be a better characteristic length scale for *Du*; as this more accurately describes current carried by EDLs. Porosimetry data indicate our pore-volume-to-surface-area ratio is order 10 nm. Using this length scale, the Mani et al. model predicts propagation at the highest buffer concentration of 1000 μM, in agreement with our observations. Full characterization of CP propagation in porous media is beyond the scope of this paper and we plan to further investigate this.

5. Conclusion

We experimentally observed propagating concentration polarization (CP) in an EO pump system. At an ionic strength of 100 μM, we observed a depletion shock with front velocity of approximately 400 μm/s (and at least 10-fold drop in ionic strength) and an enrichment front with final enrichment factor of ~1.9. We confirmed

enrichment and depletion zone propagation by measuring system conductance. Results indicate that CP propagation rate decreased with increasing initial ionic strength (increased Dukhin number), as expected from established CP theory [23]. The temporal dynamics of conductance indicated that CP fronts propagated through the entire channel.

Conductance measurements suggested CP propagated at an ionic strength of 1000 μM, which is not expected if mean pore radius is used as the characteristic length scale. We propose using pore-volume-to-surface-area ratio as the characteristic length, which for our system accurately predicts CP propagation at 1000 μM. In future work, we hope to develop models for CP propagation in porous media, where the distribution of pore-sizes introduces significant complexity.

Appendix A. Supplementary data

Supplementary data associated with this article can be found, in the online version, at doi:10.1016/j.snb.2009.10.005.

References

[1] D.J. Laser, J.G. Santiago, A review of micropumps, Journal of Micromechanics and Microengineering 14 (6) (2004) R35–R64.
[2] S.H. Yao, J.G. Santiago, Porous glass electroosmotic pumps: theory, Journal of Colloid and Interface Science 268 (1) (2003) 133–142.
[3] C.R. Buie, D. Kim, S. Litster, J.G. Santiago, An electro-osmotic fuel pump for direct methanol fuel cells, Electrochemical and Solid State LettersV 10 (11) (2007) B196–B200.
[4] S. Litster, C.R. Buie, T. Fabian, J.K. Eaton, J.G. Santiago, Active water management for PEM fuel cells, Journal of the Electrochemical Society 154 (10) (2007) B1049–B1058.
[5] L. Chen, Y. Guan, J. Ma, G. Luo, K. Liu, Application of a high-pressure electroosmotic pump using nanometer silica in capillary liquid chromatography, Journal of Chromatography A 1064 (1) (2005) 19–24.
[6] S. Litster, B. Ha, D. Kim, J.G. Santiago, A two-liquid electroosmotic pump for portable drug delivery systems, in: Proceedings of the IMECE 2007, November 11–15, Seattle, USA, 2007.
[7] A. Brask, J.P. Kutter, H. Bruus, Long-term stable electroosmotic pump with ion exchange membranes, Lab on a Chip 5 (7) (2005) 730–738.
[8] S. Yao, D.E. Hertzog, S. Zeng, J.C. Mikkelsen, J.G. Santiago, Porous glass electroosmotic pumps: design and experiments, Journal of Colloid and Interface Science 268 (1) (2003) 143–153.
[9] D. Kim, J.D. Posner, J.G. Santiago, High flow rate per power electroosmotic pumping using low ion density solvents, Sensors and Actuators A: Physical 141 (1) (2008) 201–212.
[10] C.-W. Lin, S. Yao, J.D. Posner, A.M. Myers, J.G. Santiago, Toward orientation-independent design for gas recombination in closed-loop electroosmotic pumps, Sensors and Actuators B: Chemical 128 (1) (2007) 334–339.
[11] L.X. Chen, Q.L. Li, S. Lee, J. Choo, Development of an electroosmotic pump using nanosilica particle packed capillary, IEEE Sensors Journal 8 (5–6) (2008) 488–494.
[12] Y. Takemori, S. Horiike, T. Nishimoto, H. Nakanishi, T. Yoshida, High pressure electroosmotic pump packed with uniform silica nanospheres, Solid-State Sensors, Actuators and Microsystems 2 (2005) 1573–1576.
[13] M. Suss, L. Marshall, T. Zangle, J.G. Santiago, Concentration polarization in electroosmotic pumps, ECS Transactions, in press.
[14] R.F. Probstein, Physicochemical Hydrodynamics, John Wiley & Sons, Inc., 2003.
[15] S.S. Dukhin, V.N. Shilov, Kolloidnyi Zhurnal 31 (1969) 706–713.
[16] T.A. Zangle, A. Mani, J.G. Santiago, On the propagation of concentration polarization from microchannel–nanochannel interfaces. Part II. Numerical and experimental study, Langmuir 25 (6) (2009) 3909–3916.
[17] H. Kuan-Da, Y. Ruey-Jen, A nanochannel-based concentrator utilizing the concentration polarization effect, Electrophoresis 29 (24) (2008) 4862–4870.
[18] S. Ehlert, D. Hlushkou, U. Tallarek, Electrohydrodynamics around single ion-permselective glass beads fixed in a microfluidic device, Microfluidics and Nanofluidics 4 (2009) 471–487.
[19] I. Nischang, U. Reichl, A. Seidel-Morgenstern, U. Tallarek, Concentration polarization and nonequilibrium electroosmotic slip in dense multiparticle systems, Langmuir 23 (18) (2007) 9271–9281.
[20] I. Nischang, G. Chen, U. Tallarek, Electrohydrodynamics in hierarchically structured monolithic and particulate fixed beds, Journal of Chromatography A 1109 (1) (2006) 32–50.
[21] U. Tallarek, F. Leinweber, I. Nischang, Perspective on concentration polarization effects in electrochromatographic separations, Electrophoresis 26 (2) (2005) 391–404.
[22] T. Postler, Z. Slouka, M. Svoboda, M. Pribyl, D. Snita, Parametrical studies of electroosmotic transport characteristics in submicrometer channels, Journal of Colloid and Interface Science 320 (1) (2008) 321–332.
[23] A. Mani, T.A. Zangle, J.G. Santiago, On the propagation of concentration polarization from microchannel–nanochannel interfaces. Part I. Analytical model and characteristic analysis, Langmuir 25 (6) (2009) 3898–3908.
[24] Y. Berrouche, Y. Avenas, C. Schaeffer, P. Wang, H.C. Chang, Optimization of high flow rate nanoporous electroosmotic pump, Journal of Fluids Engineering-Transactions of the ASME 130 (8) (2008).
[25] J.J. Lyklema, A.d. Keizer, B.H. Bijsterbosch, G.J. Fleer, M.A.C. Stuart, Fundamentals of Interface and Colloid Science: Electrokinetics and Related Phenomena, Academic Press, 1995.
[26] A. Persat, M.E. Suss, J.G. Santiago, Basic principles of electrolyte chemistry for microfluidic electrokinetics. Part II. Coupling between ion mobility, electrolysis, and acid–base equilibria, Lab on a Chip 9 (17) (2009) 2454–2469.

Biographies

Daniel G. Strickland is a PhD candidate in Prof. Juan G. Santiago's microfluidics research group at Stanford University. His research is on novel water management techniques for PEM fuel cells and electrokinetic phenomena in electroosmotic pumps. He received his MS in Mechanical Engineering at Stanford University and BS in Mechanical Engineering at Seattle University. His research is funded through a National Science Foundation Graduate Research Fellowship.

Matthew E. Suss received his BEng degree from McGill University, Montreal, in 2007, and MSc at Stanford University, Stanford, CA in 2009. He is currently beginning a PhD at Stanford where his research has been supported by an FQRNT fellowship and an NSERC fellowship from the Quebec and Canadian governments, respectively. His work in the Stanford Microfluidics Laboratory focuses on the development of highly efficient electroosmotic micropumps for drug delivery applications.

Thomas A. Zangle is a PhD candidate at Stanford University under the supervision of Prof. Juan G. Santiago. He received his MS in Mechanical Engineering at Stanford University, and his BE from the Thayer School of Engineering at Dartmouth College in 2005.

Juan G. Santiago is Associate Professor of Mechanical Engineering at Stanford University and Chair of the Thermosciences Group. He specializes in microscale transport phenomena and electrokinetics. He earned his PhD in Mechanical Engineering from the University of Illinois at Urbana-Champaign. Among other awards, he won the National Science Foundation Presidential Early Career Award for Scientists and Engineers (PECASE) ('03–'08). Santiago has presented 13 keynote and named lectures and over 100 additional invited lectures. His group has been awarded nine best paper and poster awards. He has authored/co-authored 98 archival publications, authored/co-authored 190 conference papers, and holds 25 patents.